remote sensing

MDPI

Article

Airborne Thermal Imagery to Detect the Seasonal Evolution of Crop Water Status in Peach, Nectarine and Saturn Peach Orchards

Joaquim Bellvert [1,2,*], Jordi Marsal [1], Joan Girona [1], Victoria Gonzalez-Dugo [3], Elías Fereres [3], Susan L. Ustin [2] and Pablo J. Zarco-Tejada [3]

Received: 7 October 2015; Accepted: 29 December 2015; Published: 5 January 2016
Academic Editors: Mutlu Ozdogan, Yoshio Inoue and Prasad S. Thenkabail

1 Efficient Use of Water Program, Institut de Recerca i Tecnologia Agroalimentàries (IRTA), Fruitcentre, Parc Cientific i Tecnològic Agroalimentari (PCiTAL), Lleida 25003, Spain; jordi.marsal@irta.es (J.M.); joan.girona@irta.es (J.G.)
2 Center of Spatial Technologies (CSTARS), Department of Land, Air and Water Resources (LAWR), University of California, Davis, CA 95616, USA; slustin@ucdavis.edu
3 Institute for Sustainable Agriculture (IAS), Consejo Superior de Investigaciones Científicas (CSIC), Alameda del Obispo, s/n, Córdoba 14004, Spain; victoria.gonzalez@ias.csic.es (V.G.-D.); ag1fecae@uco.es (E.F.); pablo.zarco@csic.es (P.J.Z.-T.)
* Correspondence: joaquim.bellvert@irta.es; Tel.: +34-902-789-449 (ext. 1566)

Abstract: In the current scenario of worldwide limited water supplies, conserving water is a major concern in agricultural areas. Characterizing within-orchard spatial heterogeneity in water requirements would assist in improving irrigation water use efficiency and conserve water. The crop water stress index (CWSI) has been successfully used as a crop water status indicator in several fruit tree species. In this study, the CWSI was developed in three *Prunus persica* L. cultivars at different phenological stages of the 2012 to 2014 growing seasons, using canopy temperature measurements of well-watered trees. The CWSI was then remotely estimated using high-resolution thermal imagery acquired from an airborne platform and related to leaf water potential (Ψ_L) throughout the season. The feasibility of mapping within-orchard spatial variability of Ψ_L from thermal imagery was also explored. Results indicated that CWSI can be calculated using a common non-water-stressed baseline (NWSB), upper and lower limits for the entire growing season and for the three studied cultivars. Nevertheless, a phenological effect was detected in the CWSI *vs.* Ψ_L relationships. For a specific given CWSI value, Ψ_L was more negative as the crop developed. This different seasonal response followed the same trend for the three studied cultivars. The approach presented in this study demonstrated that CWSI is a feasible method to assess the spatial variability of tree water status in heterogeneous orchards, and to derive Ψ_L maps throughout a complete growing season. A sensitivity analysis of varying pixel size showed that a pixel size of 0.8 m or less was needed for precise Ψ_L mapping of peach and nectarine orchards with a tree crown area between 3.0 to 5.0 m^2.

Keywords: remote sensing; peach; temperature; water status; leaf water potential; CWSI

1. Introduction

Water scarcity is a major concern in many irrigated agricultural areas of the world. Therefore, irrigation water management needs to be carried out more efficiently, aiming at saving water and maximizing its productivity [1]. The adoption of regulated deficit irrigation (RDI) techniques, using water stress indicators, has been used in many fruit trees in order to optimize water use without affecting crop yields. In peach trees (*Prunus persica* L.), the benefit is well-known for applying RDI during stage II of fruit development. Besides saving water, RDI has the potential to reduce excessive

tree vigor, maintain yield, and may improve fruit quality [2,3]. However, the difficulty in identifying spatial variability of the crop water status across orchards limits its practical implementation in commercial fields. The success of RDI techniques strongly depends on the appropriate use of on-farm irrigation system and on the capacity to use new tools to detect crop water status across orchards.

Remote sensing technologies are a successful tool to accurately identify spatial heterogeneity and have been shown to have the capacity to monitor irrigation at orchard level [4,5]. The use of remote sensing in the assessment of crop water status through canopy temperature has had a long development history. In the 1970s and 1980s, canopy temperature was first suggested as a method to detect stress using hand-held thermal infrared thermometers [6–12]. However, these measurements were site-specific and not useful to assess spatial distribution of water status within a field. The advent of modern remote sensing technologies offers the possibility to develop temperature-derived indicators from airborne thermal imaging and map spatial variability of water status.

Working on herbaceous crops, Jackson *et al.* [11] and Idso *et al.* [8] developed the concept of crop water stress index (CWSI) as a thermally base stress indicator. Since then, the CWSI has been widely used in annual crops [13–15], and more recently in perennial crops such as grapevines [16,17], olive [18,19], pistachio [20], citrus [21] and peach [22]. CWSI is inversely related to transpiration rate and stomatal conductance [7] and has been successfully related to indicators of crop water status such as leaf water potential (Ψ_L) [23,24]. However, stomatal control of canopy conductance and Ψ_L are highly sensitive to VPD, and change between cultivars and throughout crop development [25,26]. Such changes may affect the relationship between CWSI and Ψ_L. In fact, Bellvert *et al.* [27] reported significant differences in the CWSI - Ψ_L relationships between grapevine cultivars and phenological stages.

To use remotely estimates of leaf water potential (Ψ_{est}) for assessing the spatial variability in water stress across peach orchards, it would be necessary to find out the seasonal variations in the CWSI *vs.* Ψ_L relationship. The present study tested the hypothesis that Ψ_{est} is a reliable water stress indicator in different *Prunus persica* L. cultivars throughout different growing seasons, and whether there are different responses between cultivars. To achieve it, "non-water-stressed baselines", which are necessary for calculating CWSI, were developed over two seasons, and the CWSI was seasonally related with Ψ_L. The feasibility of mapping within-orchard spatial variability of Ψ_{est} from high-resolution thermal imagery, remotely acquired by an airborne platform was also explored.

2. Materials and Methods

2.1. Study Site

The study was carried out from 2012 to 2014 growing seasons in three commercial orchards located near Lleida, Spain. In 2012 and 2013, the study was carried out in a 2-ha peach (41°41′64″N, 0°32′91″E) orchard planted in 1996 with an early maturing cultivar of peach (*Prunus persica cv. Royal Glory*) in a 4 m × 3 m grid. In the same two years, results obtained in the peach orchard were validated in a 15 year old 2.2-ha nectarine orchard (*Prunus persica cv. Big Top*) planted in a 4 m × 3 m grid (41°41′72″N, 0°32′87″E). In addition, results for peach were validated in 2014 in a 3 year old 2.8-ha Saturn peach orchard (*Prunus persica cv. Platicarpa*) with tree spacing of 4 × 1.5 m grid (41°41′64″N, 0°32′38″E). Tree crown area ranged from 3.0 to 5.0 m^2 for peach and nectarine and from 1.5 to 2.5 m^2 for Saturn peach. The climate of the area is Mediterranean, with an average annual rainfall and evapotranspiration of 364 and 1088 mm, respectively. Within each orchard, three irrigation treatments were set up to test different levels of water status throughout the season. The treatments were: (i) full-irrigation control, where irrigation replaced 100% ETc; (ii) moderate deficit irrigation, where irrigation replaced 50% ETc; and (iii) deficit irrigation, where water was applied only after midday leaf water potential dropped below −2.0 MPa. Each irrigation treatment consisted of four adjacent rows with eight trees per row. The trees of the two central rows were monitored while the others served as a border. Irrigation water was applied through a drip irrigation system with emitters spaced 0.75 m apart on a single drip line

per row, discharging 8 $L \cdot h^{-1}$. Trees were irrigated daily and scheduled on a weekly basis. Water requirements were calculated using a water balance technique to replace crop evapotranspiration (ETc) as follows: ETc = (ETo × Kc)—rainfall. ETo and Kc represent the reference evapotranspiration and crop coefficient respectively. The Penmann-Monteith method was used to determine ETo (Allen *et al.*, [28]) and Kc vales were obtained from Doorenbos and Pruitt [29].

2.2. Infrared Temperature Data

Four infrared temperature sensors (IRTS) (model PC151LT-0; Pyrocouple series, Calex Electronics Limited, Bedfordshire, UK) were installed about 1.5 m above two peach trees of the full-irrigated control treatment (two sensors in each tree). Canopy temperature was measured from beginning May to mid-September for 2012 and 2013, obtaining data throughout the growing season. The calibrated IRTS were installed aiming vertically downward (nadir view). The angular field of view was 15:1 with an accuracy of ±1%, which measured a canopy target spot around 0.12 m diameter. Visual inspection of sensor positioning, comparison with air temperature (T_a) data and consistency with values measured with a hand-held infrared thermometer (Fluke 62 mini, Fluke Europe, Eindhoven, The Netherlands) ensured that 100% of the temperature signal came only from the leaves. All IRTS were connected to a datalogger (model CR200X; Campbell Scientific, Logan, UK) that recorded temperatures every minute and stored the 15-min averages. Recorded data of full-irrigated control trees was used to calculate the baselines of the crop water stress index (CWSI). The empirical CWSI was calculated as Idso *et al.* [9]:

$$CWSI = \frac{(T_c - T_a) - (T_c - T_a)_{LL}}{(T_c - T_a)_{UL} - (T_c - T_a)_{LL}} \quad (1)$$

where T_c-T_a is measured canopy-air temperature difference; $(T_c\text{-}T_a)_{LL}$ lower limit of (T_c-T_a) of a canopy which is transpiring at the potential rate, and $(T_c\text{-}T_a)_{UL}$ expected differential in the case of a non-transpiring canopy. $(T_c\text{-}T_a)_{LL}$ is function of vapour pressure deficit (VPD) (non-water-stressed baseline, NWSB). The NWSB was calculated in peach trees for two years following the procedure described in Bellvert *et al.* [17]. Only data of sunny days, which had wind speed below 6 $m \cdot s^{-1}$ (at a height of 10 m) were used in the assessment of CWSI. Hourly values of (T_c-T_a) were regressed against vapour pressure deficits (VPD) separately for the hours of the day, from 10:00 to 16:00 hours (solar time). Following recommendations of Bellvert *et al.* [17,27], the linear NWSBs were transformed to curvilinear equations to obtain the upper limits. The upper limits (UL) were obtained by solving the NWSB curvilinear equation for VPD = 0 and then correcting for vapor pressure differences caused by T_c-T_a [9]. The physical theory assigns a straight horizontal line to UL, which is irresponsive to VPD because this is only thought as dependent on relative humidity (HR). However, when different days are compared in a semi-arid climate, the VPD tends to be higher during days with high air temperature (T_a). Therefore, days with higher T_a have had higher VPD (Table 1). The UL increase with VPD reflects the effect of higher T_a on leaf energy balance. The lower limit was obtained taking the minimum values of T_c-T_a for each VPD. The NWSBs were obtained for each phenological stage: (1) stage II—lignification of endocarp (pit hardening); (2) stage III—maturation; (3) Post-harvest—from harvest (beginning July) to end of August. Stage I (considered in this study to extend from fruit set to initial pit hardening) was not studied because of low canopy cover. Pooled data from 2012 and 2013 was used to develop a common NWSB, lower and upper limits for each phenological stage and for the entire growing seasons. Air temperature (T_a), and vapor pressure deficit (VPD) were obtained from a portable weather station (Watchdog, model 2900ET, Spectrum Technologies, Inc., Plainfield, IL, USA) located on one side of the orchard, and used to obtain local meteorological conditions throughout the season.

Table 1. Climate data at the commercial orchards during the flight time.

Year	Flight Day	Stage	Orchard	T_{air} (°C)	VPD (kPa)	Rad ($W \cdot m^{-2}$)	Wind Speed (kph)
2012	14 May	II	P + N	24.0	2.4	926	6
	1 June	II	P + N	31.3	3.8	947	7
	15 June	III	P + N	32.1	3.4	959	8
	6 July	III	P + N	27.6	2.5	933	8
	31 July	PH	P + N	31.4	2.9	914	10
	21 August	PH	P + N	34.0	4.2	849	7
2013	7 May	II	P + N	24.4	1.6	904	11
	13 May	II	P + N	20.0	1.6	1052	4
	4 June	II	P + N	23.6	1.6	1083	6
	11 June	III	P + N	28.5	2.6	1082	3
	25 June	III	P + N	22.5	1.6	1078	8
	3 July	III	P + N	29.6	2.3	882	12
	16 July	PH	P + N	33.0	3.0	1032	3
	31 July	PH	P + N	33.7	3.8	1043	8
	12 August	PH	P + N	31.3	3.3	968	3
2014	30 April	II	SP	21.9	1.6	902	16
	13 May	II	SP	21.1	1.8	1050	25
	29 May	II	SP	19.7	1.0	960	4
	6 June	III	SP	28.2	1.9	1034	9
	13 June	III	SP	30.8	2.3	940	0
	27 June	III	SP	28.2	2.6	1184	0
	27 August	PH	SP	30.2	2.3	963	10

P: Peach, N: Nectarine, SP: Saturn peach.

2.3. Airborne Campaign

Flights were conducted with a thermal sensor (FLIR SC655, FLIR Systems, Wilsonville, OR, USA) installed on an aircraft (CESSNA C172S EC-JYN). The camera had a resolution of 640 × 480 pixels, equipped with a 13.1 mm optics focal length yielding an angular FOV of 45° that delivered approximate ground resolution of 0.15 to 0.20 m. The spectral response was in the range of 7.5–13 μm. The radiometric calibration of the sensor was assessed in the laboratory using a blackbody (model P80P, Land Instruments, Dronfield, UK). In addition, various calibrations were conducted at the time of each flight using surface temperature measurements to improve the calibration. The accuracy of this method is discussed in Berni *et al.* [19,30], who demonstrated an accuracy error less than 1 K using a similar camera on board an Unmanned Aerial Vehicle (UAV). The sensor was connected to a computer via USB 2.0 protocol. The software to acquire thermal images was developed at the Laboratory for Research Methods in Quantitative Remote Sensing (Quantala, IAS-CSIC, Córdoba, Spain) and described in Zarco-Tejada *et al.* [31].

The peach and nectarine orchard study sites used for field data collection can be seen in Figure 1a. The flights were conducted at 12:00 solar time (14:00 local time) at 150 m altitude above the ground level. The high-resolution thermal images enabled discrimination of pure tree crowns from soil background effects (Figure 1b). The flying pattern consisted of four longitudinal lines of 1500 m separated by 65 m. Table 1 lists imagery acquisition dates, phenological stages and weather conditions for each flight throughout the growing season. Concomitant with each flight, leaf water potential (Ψ_L) was measured in 18 trees in each orchard (six per irrigation treatment). Two fully expanded leaves exposed to direct sunlight were measured on each tree. A Scholander pressure chamber (Soil Moisture Equipment Corp., Santa Barbara, CA, USA) was used following the recommendations of Turner and Long [32]. Aluminum foil was used between rows as a target to mark the exact location of measured trees. Mean crown temperature (T_c) was extracted from six trees per irrigation treatment and used to calculate the crop water stress index (Figure 1c).

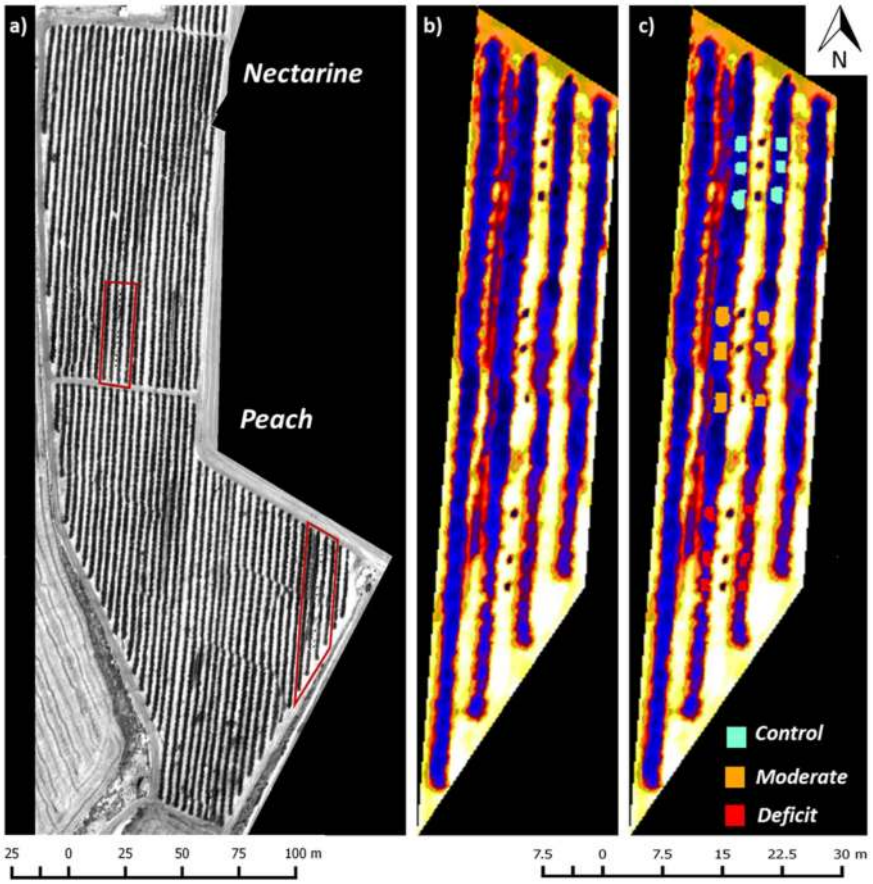

Figure 1. Thermal mosaic acquired at 0.20 m pixel resolution, observing in (**a**) nectarine and peach orchards. In red are shown the areas where the irrigation treatments were located; (**b**) detailed study site area used for field data collection in the peach orchard. Trees under different irrigation treatments (full-irrigation control, moderate and deficit irrigation) were measured and located with aluminium foil between rows; and (**c**) peach trees under different irrigation treatments used for pure tree crown temperature extraction.

Simultaneously with each flight in 2013, stomatal conductance (g_s) was also measured in the nectarine orchard using a steady-state porometer (model LI-1600, Li-Cor Inc., Lincoln, NE, USA). g_s was measured in the same leaves where Ψ_L was recorded.

2.4. Spatial Resolution Assessment

The influence of pixel size on crop water status detection was studied for determining the minimum and best possible spatial resolution that may be required in assessing T_c of peach and nectarine trees. The thermal imagery acquired on 1 and 15 June 2012 were re-sampled using a pixel aggregate technique through cubic convolution. Newly obtained re-sampled images had pixel sizes of 0.3, 0.6, 1.0, 1.2, 1.5, and 2.0 m. Exactly the same region of interest created for the eighteen peach and nectarine trees for the very high resolution thermal imaging was used to extract the aggregated pixels from the lower resolution mosaics.

2.5. Estimation of Ψ_L from CWSI and Validations

Estimation of leaf water potential for peach trees was performed comparing two methods: (1) using CWSI for each specific phenological stage; and (2) using a common CWSI pooling data from two consecutive growing seasons. In addition, the methodology proposed to estimate Ψ_L in peach trees

was also validated for nectarine and Saturn peach trees in different years. The "non-water-stressed baselines" developed for peach trees were then also used to calculate CWSI for these two cultivars.

2.6. Statistical Analysis

Non-watered-stressed baselines (NWSB) were transformed to a linear regression model for the purpose of analyzing differences between phenological stages. A covariance analysis (ANCOVA) was performed to analyze differences between years and phenological stages using the SAS statistical package [33]. Specific differences among phenological stages in the slopes and intercept of the lines were subsequently tested by orthogonal contrasts.

3. Results

3.1. Non-Water-Stressed Baselines

The relationship between difference of canopy and air temperature (T_c-T_a) with vapor pressure deficit (VPD) for well-watered peach trees was significant for the two years of study (Figure 2). The T_c-T_a trend decreased as VPD increased. The coefficients of determination (R^2) ranged from 0.61 to 0.85. Although not significant differences were detected between years during stages II and III, the differences in the post-harvest stage were significant. During post-harvest, the intercept in the T_c-T_a *vs.* VPD relationship was significantly higher in 2012 than in 2013. However, a common baseline using the two years of data was performed for each phenological stage. The statistical analysis indicated a different phenological response within years (Table 2). The intercept of the relationship T_c-T_a *vs.* VPD was significantly different for two studied years ($p < 0.0001$). In 2012, T_c-T_a *vs.* VPD relationship from stage II presented a higher intercept than stage III. On the other hand, the intercept of post-harvest stage in 2013 was significantly lower in comparison with earlier stages. In the same year, the phenological stage III had the lowest slope and post-harvest had the highest.

Table 2. A covariance analysis (ANCOVA) analysis of T_c-T_a for phenological stages at different years and probabilities tested by orthogonal contrasts of slopes (Stage × vapour pressure deficit (VPD)) and intercepts (Stage).

	2012	**2013**		**All Years**
VPD	<0.0001 *	<0.0001 *		<0.0001 *
Stage	<0.0001 *	<0.0001 *		<0.0001 *
Stage × VPD	0.957	<0.0001 *		0.0641
Contrast **	**Stage**	**Stage**	**Stage × VPD**	**Stage**
Stage II *vs.* III	0.0414	-	0.0451	0.0197
Stage II *vs.* PH	-	0.0059	<0.0001	0.0431
Stage III *vs.* PH	-	<0.0001	<0.0001	-

* Significance at $p < 0.0001$ (SAS 2002); ** Significance at $p < 0.05$ (SAS 2002).

The T_c-T_a *vs.* VPD relationships were used to develop the curvilinear NWSBs, and lower and upper limits for each phenological stage and for the entire growing season (Figure 3). It is interesting to emphasize that LL and UL of stage III had a slightly different slope and intercept in comparison with other stages, perhaps related to a higher T_a and global solar radiation during that period. These differences were considered negligible and a common LL and UL was used for the entire growing season (Figure 3c).

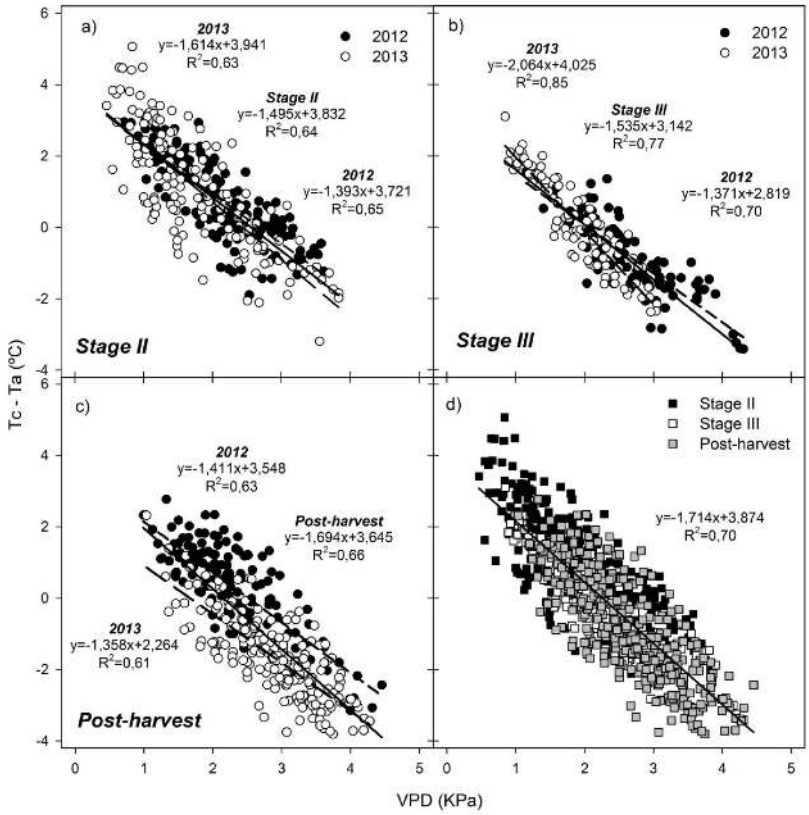

Figure 2. Relationships between the difference of canopy and air temperature (T_c-T_a) and vapour pressure deficit (VPD) for the 10:00 to 16:00 hour data of fully irrigated control peach trees, showing: (**a**–**c**) differences between years (2012 and 2013) at different phenological stages (Stages II and III, and post-harvest); and (**d**) seasonal response for two years data. All relationships were significant ($p < 0.0001$).

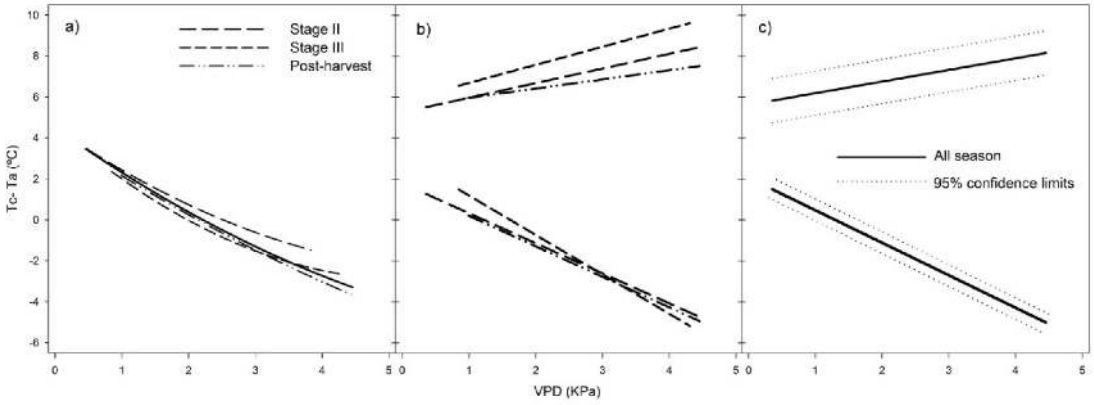

Figure 3. (**a**) Non-water-stressed baselines (NWSB), and (**b**) lower and upper limits, used to calculate the CWSI for peach trees at different phenological stages (Stages II and III, Post-harvest) and (**c**) for the entire growing season (All Season). All relationships were significant ($p < 0.0001$).

3.2. Relationship between CWSI and Ψ_L for Peach Trees

Midday Ψ_L correlated significantly with CWSI for the entire growing season and followed a curvilinear model during pre-harvest stages and a linear model during post-harvest (Figure 4). This means that during pre-harvest, ΨL started to decline significantly only after a threshold CWSI value.

A significant seasonal effect was also observed in this relationship, indicating that for a particular level of CWSI, the values of Ψ_L were lower as the crop developed.

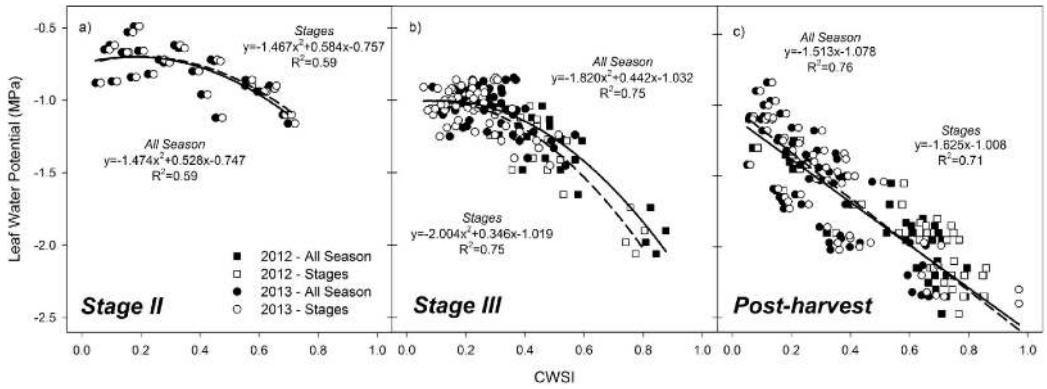

Figure 4. (**a**–**c**) Comparison of the relationship between crop water stress index (CWSI) and leaf water potential (Ψ_L) for peach trees at different phenological stages of the 2012 and 2013 growing seasons. CWSI has been calculated using the lower and upper limits for each specific phenological stage (*Stages*) and for all the season (*All Season*). All relationships were significant ($p < 0.0001$).

CWSI was calculated under two different methods: (i) using baselines (lower and upper limits) for each phenological stage; and (ii) using a common baseline for the entire growing season. Visually, the two methods had similar responses without differences in the functions and coefficients of determination (R^2) (Figure 4). In order to identify which method had the strongest influence on Ψ_L estimation, Ψ_L was estimated using both methods and related to the observed Ψ_L by linear regression. The one-to-one relationships between estimated and observed Ψ_L were significant for all phenological stages ($p < 0.0001$), and no significant differences were found between methods used for estimating Ψ_L (Figure 5). There were differences in the one-to-one relationships at different phenological stages. Despite the regression from stage II having the lowest root mean square error (RMSE), it also presented a low slope and high intercept. Stage III had a higher RMSE than stage II, but the intercept was closer to zero and the slope to one. Although intercept and slope of regressions from the post-harvest stage were similar to stage III, the RMSE was higher (Figure 5c,g). The best fit regression was obtained taking into account data from the entire season (Figure 5d,h). This comparison was done for peach trees using data from two consecutive years, and showed that the CWSI *vs.* Ψ_L relationships in 2012 agreed with those of 2013.

3.3. Validation for Nectarine and Saturn Peach

The algorithms of CWSI developed for peach trees were validated for nectarine and Saturn peach trees. The seasonal relationships between midday Ψ_L and CWSI for nectarine and Saturn peaches followed the same trend as those of peach trees (Figure 6). Coefficients of determination ranged from 0.52 to 0.78 and were similar to those presented in Figure 4 for peach trees. Estimates of leaf water potential using seasonal pooled data from all cultivars fitted significantly well with observed Ψ_L ($p < 0.0001$) (Figure 7). However, differences in their slopes and intercepts were detected in comparison with estimates of Ψ_L only using peach tree data. The regression at stage II had the lowest R^2 and slope and a high intercept (Figure 7a). In Stage III, despite the RMSE was 0.20 MPa, the slope and intercept of the regression were respectively closer to one and zero in comparison with the same regression only with peach tree data (Figure 7b). The pertinent regressions from post-harvest and all season had a slight decrease in the adjusted one-to-one parameters in comparison with those presented in Figure 3 at their respective stages (Figure 7c,d). Overall, despite a slight decrease in the one-to-one regressions with data from all three cultivars in comparison with only data from peach trees, it seems that estimates of Ψ_L are robust throughout the season.

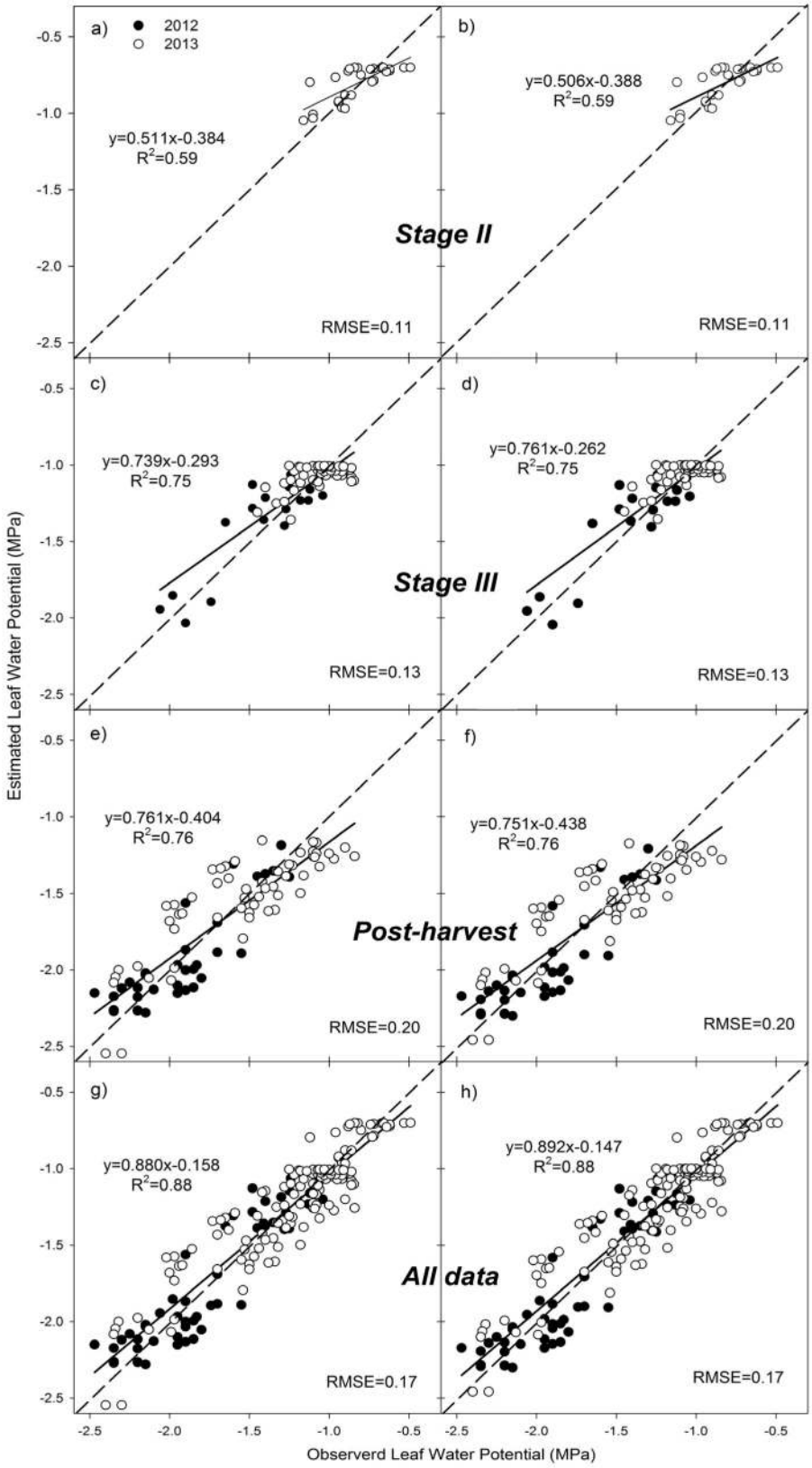

Figure 5. (**a**–**h**) Relationships between observed and estimated Ψ_L for peach trees at different phenological stages of the 2012 and 2013 growing seasons. Estimated Ψ_L has been obtained from the calculation of CWSI using: (**left**) a common equation for all the season; and (**right**) equations for each phenological stage. All relationships were significant ($p < 0.0001$).

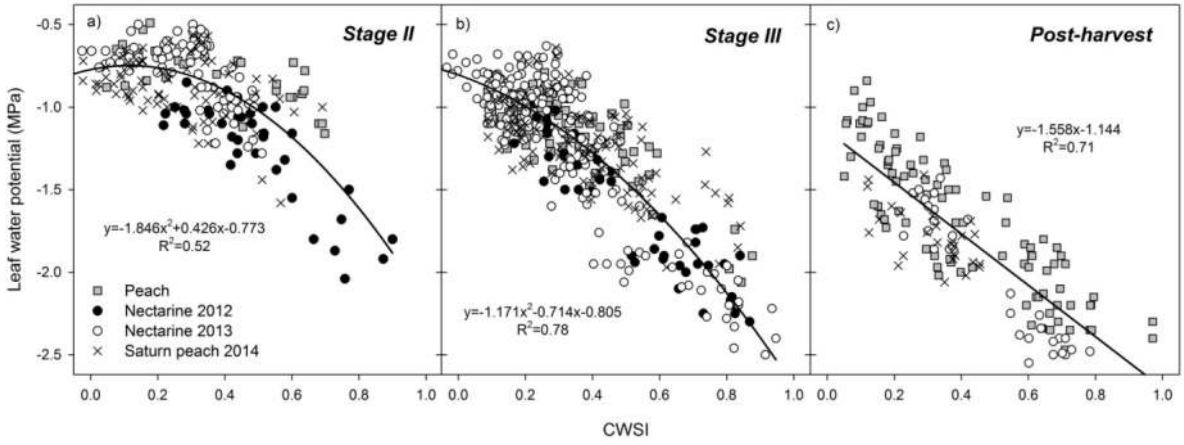

Figure 6. (**a**–**c**) Seasonal validation of the relationship between CWSI and leaf water potential (Ψ_L) in nectarine for the 2012 and 2013 growing season and Saturn peach trees for 2014 growing season. Data obtained for peach trees has been added as standard comparison. All relationships were significant ($p < 0.0001$).

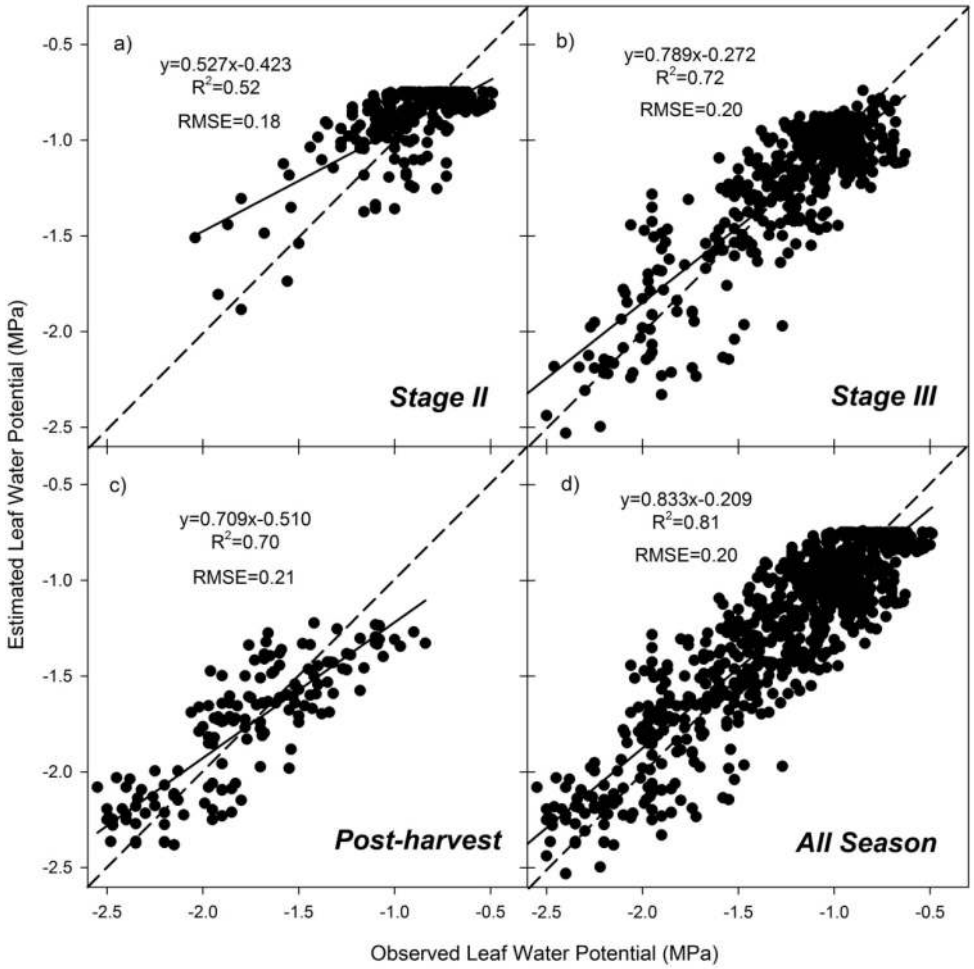

Figure 7. (**a**–**d**) Relationships between observed and estimated Ψ_L for peach, nectarine and Saturn peaches at different phenological stages using data from 2012 to 2014 growing seasons. All relationships were significant ($p < 0.0001$).

3.4. Minimum Pixel Size to Detect Water Stress

High resolution thermal imagery enabled the retrieval of pure tree crown pixels, while lower spatial resolution has more chances to contain pixels with mixed information of canopy, shadows and soil background, making it difficult to remotely estimate Ψ_L with sufficient precision.

The relationship between Ψ_L and CWSI tend to reduce R^2 with increasing pixel size (Table 3). Thermal mosaics with a pixel size of 0.15 and 0.30 m had the highest R^2. Also, the regressions between measured and estimated Ψ_L for peaches and nectarines were well adjusted and had the lowest RMSE. Contrary to results provided by Bellvert *et al.* [17] in grapevines, which indicated that a minimum pixel size of 0.30 m was the optimum, it seems that for peach and nectarine trees, pixel size can be higher. Pixel sizes from 0.60 to 0.80 m almost had not a negative effect on R^2, and the RMSE for those pixel sizes only increased around 6% in comparison with pixels at 0.30 m. On the other hand, despite pixels at 1.00 m pixel size having a significant relationship, the RMSE was too high. There was no significant relationship between Ψ_L and CWSI from 1.20 m resolution.

Table 3. Comparison of the coefficients of determination (R^2) of the relationship between Ψ_L (y) and CWSI (x) for grapevines obtained by Bellvert *et al.* [17] and peach and nectarine trees at different spatial pixel resolutions ranging from 0.15 to 2.00 m. R^2 for peach and nectarine trees corresponded with data from thermal images acquired on 1 and 15 June 2012. Ψ_{est} (y) from the Ψ_L *vs.* Ψ_{est} regression was estimated from the equation corresponding with stage III ($\Psi_{est} = -1.171CWSI^2 - 0.714CWSI - 0.805$).

Grapevines	**Peaches & Nectarines**				
		Ψ_L ***vs.* CWSI**		Ψ_L ***vs.* Ψ_{est}**	
Pixel Size (m)	**R^2**	**R^2**	**Equation**	**Equation**	**RMSE**
0.15	-	0.76 *	$y = -1.708\ x^2 + 0.194x - 0.993$	$y = 0.905x - 0.263$	0.21
0.30	0.71	0.75 *	$y = -1.669\ x^2 + 0.252x - 1.060$	$y = 0.942x - 0.187$	0.21
0.60	0.38	0.66 *	$y = -0.573\ x^2 - 0.707x - 0.883$	$y = 0.986x - 0.147$	0.27
0.80	0.27	0.65 *	$y = -0.249\ x^2 - 0.979x - 0.850$	$y = 1.053x - 0.044$	0.28
1.00	0.22	0.56 *	$y = -0.224\ x^2 - 0.743x - 0.908$	$y = 1.204x - 0.009$	0.46
1.20	<0.10	0.28	$y = -0.742x - 0.997$	$y = 0.808x - 0.586$	0.56
1.50	0.28	0.11	$y = -0.468x - 1.089$	$y = 0.651x - 1.143$	0.88
2.00	0.29	<0.10	-	-	-

* Relationships were significant at $p = 0.05$ (SAS 2002).

3.5. Maps of Remotely Estimated Ψ_L

The information developed in this study enables the generation of maps of remotely sensed leaf water potential (Ψ_{est}) throughout a complete growing season. To carry this out successfully, the seasonal relationships reported in this study must be taken into account. Figure 8 shows Ψ_{est} maps of the peach and nectarine orchards at different phenological stages in the 2013 growing season. The farmer applied two different irrigation strategies in different irrigation sectors: (i) Control, full-irrigation throughout the growing season; and (ii) Regulated Deficit Irrigation (RDI), which consisted on applying mild deficit irrigation during stage II and severe deficit during post-harvest. During stage III, both irrigation sectors were fully irrigated. Ψ_{est} maps illustrated the spatial variability across the orchard and the differences in crop water status between irrigation sectors. For instance, those irrigation sectors under RDI had lower Ψ_{est} during stage II and post-harvest than the Controls.

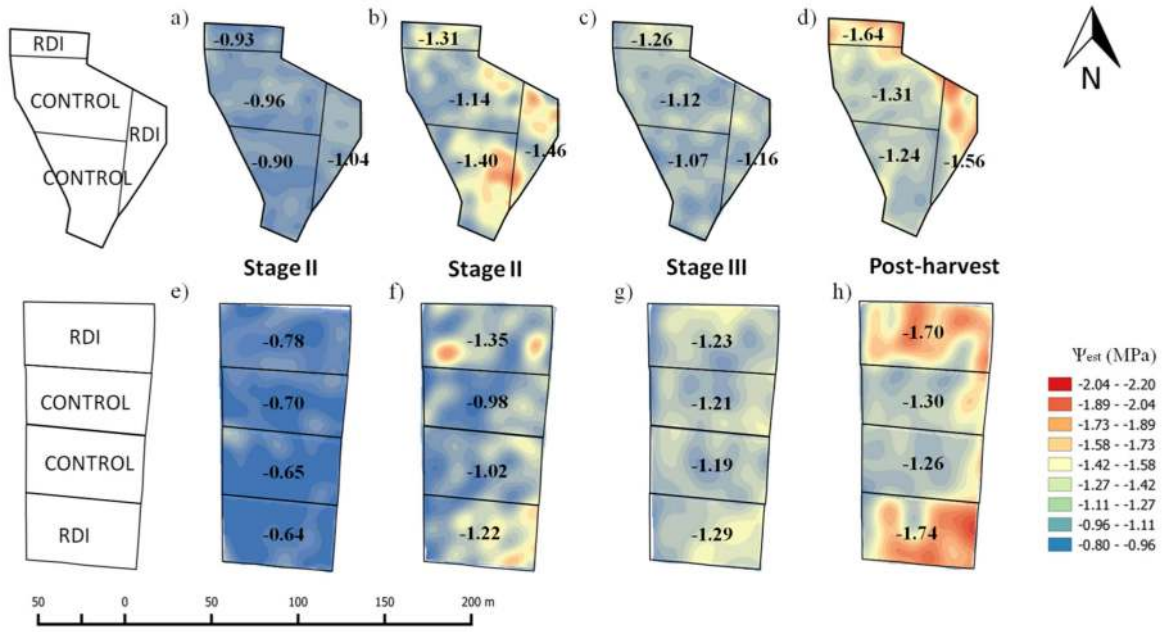

Figure 8. Maps of remotely sensed leaf water potential (Ψ_{est}) at different phenological stages of the 2013 growing season for a 2-ha peach (**a**–**d**) and 2.2-ha nectarine orchard (**e**–**f**). Two different irrigation treatments were applied at irrigation sector level (full irrigation, CONTROL) and Regulated Deficit Irrigation (RDI). Averaged Ψ_{est} values for each irrigation sector are indicated. The equations applied to estimate Ψ_{est} from CWSI were the following: $y = -1.846x^2 + 0.426x - 0.773$ (stage II), $y = -1.171x^2 - 0.714 - 0.805$ (stage III), and $y = -1.558x - 1.144$ (post-harvest).

4. Discussion

To our knowledge, studies that published NWSB in heterogeneous crop surfaces are scarce. A linear NWSB was developed in this study for peach trees using all season data of two following years (Figure 2d). This NWSB was similar to those reported for other crops such as olive and sweet lime trees, but completely different than other crops (Table 4 [5,20,21,34–37]). Mandarine and orange trees were the only crops that reported a higher intercept of the NWSB than peach trees [21]. Therefore, it seems that well-watered peach trees displayed a lower transpiration rate than most other crops, leading an increase in T_c-T_a at a given VPD.

Table 4. Parameters of the NWSB (T_c-T_a = a· VPD + b) for different heterogeneous crops.

Species	Cultivar	a	b	Reference
Peach	Royal Glory	−1.71	3.87	This study
Nectarine	Independence	−1.69	0.68	[34]
Apple	Royal Gala	−3.90	1.00	[35]
Sweet lime	Swing	−1.74	3.61	[36]
Pistachio	Kerman	−1.33	2.44	[20]
Olive	Arbequina	−2.05	3.97	[37]
Mandarin	Clemenvilla	−0.50	4.06	[21]
Orange	Powell	−0.38	4.58	[21]
Grapevines	Chardonnay	−1.39	2.16	[5]

The relationship between T_c-T_a and VPD for well-watered peach trees presented a slightly different phenological response due to the higher intercept in the stage II regression (Figure 2). This implied that for a given increase in VPD, stage II had less transpirational cooling than stages III and post-harvest. Morphological and hydraulic consideration on trees can explain part of these

seasonal differences. For instance, it is well-known that maximum transpiration rates occurs just before harvest, especially during the period of rapid fruit growth, and then drops off after the fruit has been removed [38]. Despite this, we did not detect different responses between stage III and post-harvest in the relationship T_c-T_a *vs.* VPD. Differences in water use may explain the dissimilarities between stages II and III. However, despite significance in the phenology, differences were not very large and did not have a negative effect on the estimation of CWSI. In fact, the relationships between CWSI and Ψ_L at different phenological stages exhibited the same response either taking into account different NWSB for each phenological stage or a common NWSB for the entire season (Figure 4). This means that CWSI for peach trees can be easily estimated throughout a growing season using the same lower and upper limits and without considering the phenological stage.

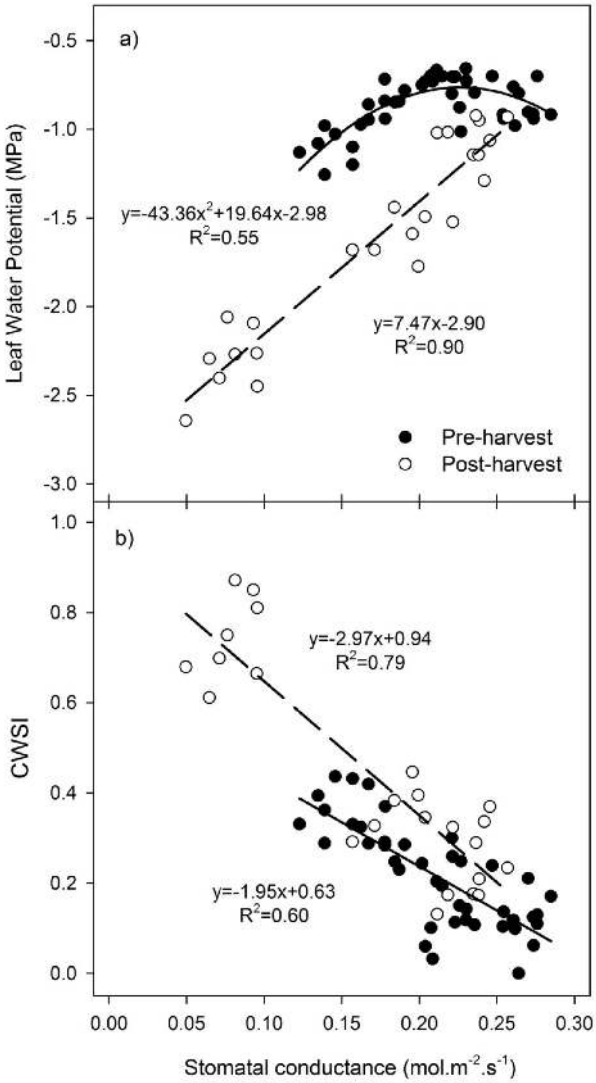

Figure 9. Relationship between stomatal conductance and (**a**) leaf water potential (Ψ_L) and; (**b**) CWSI in nectarines throughout the 2013 growing season. All relationships were significant ($p < 0.0001$).

A phenological effect was detected in the CWSI *vs.* Ψ_L relationships (Figure 4). These differences may depend on osmotic potential and leaf turgor seasonal changes. Marsal *et al.* [26] reported phenological differences for peach trees in osmotic leaf water potential at turgor loss point ($\Psi_\pi{}^\circ$), and osmotic potential at full turgor ($\Psi_\pi{}^{100}$). Both, $\Psi_\pi{}^\circ$ and $\Psi_\pi{}^{100}$ trend to decrease as crops developed. Therefore, this hypothesis may explain the phenological differences detected in the relationship between CWSI and Ψ_L, where for a specific CWSI value, Ψ_L was more negative as the crop developed

(Figure 4). A similar behavior was also reported in grapevines by Bellvert *et al.* [27]. In contrast to post-harvest, the pre-harvest CWSI *vs.* Ψ_L relationships were curvilinear. This indicates a lower Ψ_L sensitivity to CWSI in pre-harvest than in post-harvest stages. The reason for this curvature initiation is due in part to progressive stomatal closure in response to Ψ_L at early stages. In fact, there was a clear distinction between Ψ_L influences on stomatal conductance (g_s) in the different phenological stages (Figure 9a). The relationship between Ψ_L and g_s shows a progressive decrease in Ψ_L from a certain threshold of g_s at pre-harvest stages (stages II and III), while it is linear at post-harvest. The same level of g_s, corresponded to lower Ψ_L values at post-harvest than at pre-harvest stages. This indicated a higher control of water loss during pre-harvest stages than post-harvest, which seems consistent with the phenological sensitivity of g_s to Ψ_L. Ψ_L at turgor loss from water (when g_s approaches zero) approached levels of −3.0 and −2.9 MPa respectively for pre- and post-harvest stages. These values are in agreement with those reported by Marsal *et al.* [26] in peaches. The relationship between CWSI and g_s also indicated a different phenological response (Figure 9b). A specific g_s corresponded with lower CWSI values at pre-harvest than post-harvest stage. It has been reported that fruit removal significantly decreases the net photosynthesis rate, stomatal conductance and transpiration rate, and increased leaf temperature around midday [39]. Therefore, the higher CWSI values of post-harvest can be explained because of the reduction on the transpiration rate and thereby leaf evaporative cooling.

4.1. Validations with Nectarine and Saturn Peach

One goal of this research was to find out if the relationship between CWSI and Ψ_L had the same response among peach cultivars. This regression was also validated for nectarine in 2012 and 2013 and for Saturn peach in 2014. Figure 6 shows that data collected for nectarine in two years agreed with the seasonal CWSI-Ψ_L relationships of peach trees. Also, data of Saturn peaches followed the same pattern. Although a slight decrease in the R^2 was detected when data for three cultivars was pooled in comparison to using only data for peach trees, the relationships were significant and R^2 ranged from 0.52 (stage II) to 0.78 (stage III) (Figure 6). Therefore, it seems that contrary to grapevines, where differences between cultivars were detected [27], a common algorithm for each specific phenological stage can be used to estimate Ψ_L in the three peach cultivars.

The one-to-one relationships between estimated and observed Ψ_L were again plotted using the common algorithms for the three peach cultivars (Figure 7). Generally, despite these regressions being less well fitted to 1:1 than the peach tree data (Figure 5), differences were not significant. The corresponding regression of stage II had the poorest fitting (Figure 7a). It seems that Ψ_L values above −1.0 MPa were difficult to estimate. This is because the CWSI-Ψ_L relationship at stage II is curvilinear and there is little response of Ψ_L to changes of CWSI below the threshold of 0.3 (Figure 6). This might make it difficult to estimate Ψ_L for well-watered peaches during the early season. The RMSE between observed and estimated Ψ_L at different phenological stages ranged from 0.18 to 0.21 MPa. However, it seems that the RMSE had a different response depending on Ψ_L, where trend to decrease as Ψ_L was higher (Table 5). The overall relationship between averaged Ψ_L and RMSE for flights from all three years was significant with a R^2 of 0.91.

Table 5. Relationship between the Root Mean Square Error (RMSE) between observed and estimated leaf water potential at different leaf water potential (Ψ_L) ranges for the three *Prunus persica* L. cultivars.

Ψ_L Range (MPa)	RMSE
−2.0 to −2.6	0.26
−1.6 to 1.9	0.25
−1.3 to −1.8	0.22
−1.0 to −1.2	0.18
−0.6 to −0.9	0.18

4.2. Minimum Pixel Size for Water Stress Detection

One of the limitations to successfully detect crop water status through thermal imagery is the pixel size. In grapevines, it was demonstrated that the minimum pixel size is at least 0.30 m [17]. However, canopy area and width of grapevines is much less than in stone fruit trees. Therefore, it was expected that peach and nectarine water status could be remotely detected at poorer spatial resolutions. The results indicated that, in peach and nectarine trees such as those from this study (tree crown area between 3.0 to 5.0 m^2), it is necessary to obtain thermal images of at least 0.80 m pixel size (Table 3). However, it is also important to mention that the accuracy increases as the pixel size decreases.

4.3. Monitoring Irrigation Based on Crop Water Status Maps

This study demonstrated that CWSI is a suitable indicator for water status monitoring in peach and nectarine orchards in semi-arid conditions, and also for manage irrigation in precision agriculture. The acquisition of Ψ_{est} maps for an entire growing season allowed farmers to identify spatial differences in terms of water status and to carry out a more efficient differential irrigation management by either identifying sensitive areas or by setting different thresholds for irrigation. It has also been demonstrated that the adoption of RDI strategies can generate considerable water savings without having a negative impact on yield. Therefore, the use of remotely sensed maps of Ψ_{est} appears as a valuable tool for implementing RDI strategies in commercial orchards.

5. Conclusions

It was concluded that CWSI derived from remotely sensed thermal imagery is a suitable indicator for water stress monitoring in peach species. This study demonstrated that calculation of CWSI in *Prunus Persica* L. cultivars has not a different seasonal response and a common "non-water-stressed baseline" can be used throughout the growing season. However, for remote estimations of Ψ_L it is necessary to take into account the different seasonal CWSI-Ψ_L response. It is also important to underline that estimations of Ψ_L are robust for different growing seasons and that it has the same response in the three studied *Prunus persica* L. cultivars. Therefore, the applicability of these results are presented as a promising and powerful tool for assessing variability of crop water stress in heterogeneous crop orchards.

Acknowledgments: The funding of this research came from the Spanish Ministry of Economy and Competitiveness, under Project INNPACTO IPT-2011-1786-060000. We are grateful to Codorniu winery and Sorigué, S.A. for their support in this study. We thank RS Aviation, and in particular Mr Robert Pedra for his contribution to the acquisition of images. Technicians from the Efficient Use of Water program in IRTA and Quantalab (IAS-CSIC) are also acknowledged for their technical support in the field campaigns.

Author Contributions: All authors from IRTA and IAS-CSIC contributed to developing the overall research concept and data interpretations. Pablo J. Zarco-Tejada processed the image collections. Joaquim Bellvert collected and analyzed field data, as well as wrote the majority of the manuscript with contributions from all the remaining authors. Susan L. Ustin contributed in the final revisions of the manuscript.

Conflicts of Interest: The authors declare no conflict of interest.

References

1. Fereres, E.; Soriano, M.A. Deficit irrigation for reducing agricultural water use. *J. Exp. Bot.* **2007**, *58*, 147–159. [CrossRef] [PubMed]
2. Behboudian, M.H.; Marsal, J.; Girona, J.; Lopez, G. Quality and yield responses of deciduous fruits to reduced irrigation. *Hort. Rev.* **2011**, *38*, 149–189.
3. Lopez, G.; Behboudian, M.H.; Echeverria, G.; Girona, J.; Marsal, J. Instrumental and sensory evaluation of fruit quality for "Ryan's sun" peach grown under deficit. *Irrig. Hort. Technol.* **2011**, *21*, 712–719.
4. Sepulcre-Cantó, G.; Zarco-Tejada, P.J.; Jimenez-Muñoz, J.; Sobrino, J.; de Miguel, E.; Villalobos, F.J. Detection of water stress in a olive orchard with thermal remote sensing imagery. *Agric. For. Meteorol.* **2006**, *136*, 31–44.

5. Bellvert, J.; Zarco-Tejada, P.J.; Marsal, J.; Girona, J.; González-Dugo, V.; Fereres, E. Vineyard irrigation scheduling based on airborne thermal imagery and water potential thresholds. *Aust. J. Grape Wine Res.* **2015**. [CrossRef]
6. Tanner, C.B. Plant temperatures. *Agron. J.* **1963**, *55*, 210–211. [CrossRef]
7. Fuchs, M.; Tanner, C.B. Infrared thermometry of vegetation. *Agron. J.* **1966**, *58*, 297–601. [CrossRef]
8. Idso, S.B.; Jackson, R.D.; Reginato, R.J. Extending the degree day concept of plant phenological development to include water stress effects. *Ecology* **1978**, *59*, 431–433. [CrossRef]
9. Idso, S.B.; Jackson, R.D.; Pinter, P.J.; Reginato, R.J.; Hatfield, J.L. Normalizing the stress-degree day parameter for environmental variability. *Agric. Meteorol.* **1981**, *24*, 45–55. [CrossRef]
10. Jackson, R.; Reginato, R.; Idso, S.B. Wheat canopy temperature: A practical tool for evaluating water requirements. *Water Resour. Res.* **1977**, *13*, 651–656. [CrossRef]
11. Jackson, R.; Idso, S.; Reginato, R.; Pinter, P.J. Canopy temperature as a crop water stress indicator. *Water Resour. Res.* **1981**, *17*, 1133–1138. [CrossRef]
12. Jackson, R. Canopy temperature and crop water stress. *Adv. Irrig.* **1982**, *1*, 43–85.
13. Wanjura, D.F.; Hatfield, J.L.; Upchurch, D.R. Crop water stress index relation-ships with crop productivity. *Irriig. Sci.* **1990**, *11*, 93–99.
14. Irmak, S.; Haman, D.Z.; Bastug, R. Determination of crop water stress index for irrigation timing and yield estimation of corn. *Agron. J.* **2000**, *92*, 1221–1227. [CrossRef]
15. Kar, G.; Kumar, A. Surface energy fluxes and crop water stress index in ground-nut under irrigated ecosystem. *Agric. For. Meteorol.* **2007**, *146*, 94–106. [CrossRef]
16. Möller, M.; Alchanatis, V.; Cohen, Y.; Meron, M.; Tsipris, J.; Naor, A.; Ostrovsky, V.; Sprintsin, M.; Cohen, S. Use of thermal and visible imagery for estimating crop water status of irrigated grapevine. *J. Exp. Bot.* **2007**, *58*, 827–838. [CrossRef] [PubMed]
17. Bellvert, J.; Zarco-Tejada, P.J.; Girona, J.; Fereres, E. Mapping crop water stress index in a "Pinot-noir" vineyard: Comparing ground measurements with thermal remote sensing imagery from an unmanned aerial vehicle. *Precis. Agric.* **2014**, *15*, 361–376. [CrossRef]
18. Ben-Gal, A.; Agam, N.; Alchanatis, V.; Cohen, Y.; Yermiyahu, U.; Zipori, I.; Presnov, E.; Sprintsin, M.; Dag, A. Evaluating water stress in irrigated olives: Correlation of soil water status, tree water status, and thermal imagery. *Irrig. Sci.* **2009**, *27*, 367–376. [CrossRef]
19. Berni, J.J.; Zarco-Tejada, P.J.; Sepulcre-Cantó, G.; Fereres, E.; Villalobos, F. Mapping canopy conductance and CWSI in olive orchards using high resolution thermal remote sensing imagery. *Remote Sens. Environ.* **2009**, *113*, 2380–2388. [CrossRef]
20. Testi, L.; Goldhamer, D.A.; Iniesta, F.; Salinas, M. Crop water stress index is a sensitive water stress indicator in pistachio trees. *Irrig. Sci.* **2008**, *26*, 395–405. [CrossRef]
21. Gonzalez-Dugo, V.; Zarco-Tejada, P.J.; Fereres, E. Applicability and limitations of using the crop water stress index as an indicator of water deficits in citrus orchards. *Agric. For. Meteorol.* **2014**, *198–199*, 94–104. [CrossRef]
22. Wang, D.; Gartung, J. Infrared canopy temperature of early-ripening peach trees under postharvest deficit irrigation. *Agric. Water Manag.* **2010**, *97*, 1787–1794. [CrossRef]
23. Cohen, Y.; Alchanatis, V.; Meron, M.; Saranga, Y.; Tsipis, J. Estimation of leaf water potential by thermal imagery and spatial analysis. *J. Exp. Bot.* **2005**, *417*, 1843–1852. [CrossRef] [PubMed]
24. Gonzalez-Dugo, V.; Zarco-Tejada, P.J.; Nicolás, E.; Nortes, P.A.; Alarcón, J.J.; Intrigliolo, D.S.; Fereres, E. Using high resolution UAV thermal imagery to assess the variability in the water status of five fruit tree species within a commercial orchard. *Precis. Agric.* **2013**, *14*, 660–678. [CrossRef]
25. McCutchan, H.; Shackel, K. Stem-water potential as a sensitive indicator of water stress in prune trees (*Prunus domestica* L. *cv.* French). *J. Am. Soc. Hortic. Sci.* **1992**, *117*, 607–611.
26. Marsal, J.; Girona, J. Relationship between leaf water potential and gas exchange activity at diferent phenological stages and fruit loads in peach trees. *J. Am. Soc. Hortic. Sci.* **1997**, *122*, 415–421.
27. Bellvert, J.; Zarco-Tejada, P.J.; Girona, J.; Marsal, J.; Fereres, E. Seasonal evolution of crop water stress index in grapevine varieties determined with high resolution remote sensing thermal imagery. *Irrig. Sci.* **2015**, *33*, 81–93. [CrossRef]
28. Allen, R.G.; Pereira, L.S.; Raes, D.; Smith, M. *Crop Evapotranspiration. Guidelines for Computing Crop Water Requirements*; FAO Irrigation and Drainage Paper No. 56; FAO: Rome, Italy, 1998.

29. Doorenbos, J.; Pruitt, W. *Guidelines for Predicting Crop Water Requirements*; FAO Irrigation and Drainage Paper No. 24; FAO: Rome, Italy, 1977; p. 144.
30. Berni, J.A.; Zarco-Tejada, P.J.; Suarez, L.; Fereres, E. Thermal and narrow-band multispectral remote sensing for vegetation monitoring from an unmanned aerial vehicle. *IEEE Trans. Geosci. Remote Sens.* **2009**, *47*, 722–738. [CrossRef]
31. Zarco-Tejada, P.J.; González-Dugo, V.; Berni, J.A.J. Fluorescence, temperature and narrow-band indices acquired from a UAV platform for water stress detection using a micro-hyperspectral imager and a thermal camera. *Remote Sens. Environ.* **2012**, *117*, 322–337. [CrossRef]
32. Turner, N.C.; Long, M.J. Errors arising from rapid water loss in the measurement of leaf water potential by pressure chamber technique. *Aust. J. Plant Physiol.* **1980**, *7*, 527–537. [CrossRef]
33. SAS. *Enterprise Guide Version 4.2*; SAS Institute Inc.: Cary, NC, USA, 2002.
34. Tormann, H. Canopy temperature as a plant water stress indicator for nectarines. *S. Afr. J. Plant Soil* **1986**, *3*, 110–114. [CrossRef]
35. Andrews, P.K.; Chalmers, D.J.; Moremong, M. Canopy-Air temperature differences and soil water as predictors of water stress of apple trees grown in a humid, temperate climate. *J. Am. Soc. Hortic. Sci.* **1992**, *117*, 453–458.
36. Sepaskhah, A.R.; Kashefipour, S.M. Relationships between leaf water potential, CWSI, yield and fruit quality of sweet lime under drip irrigation. *Agric. Water Manag.* **1994**, *25*, 13–22. [CrossRef]
37. Bellvert, J.; Zarco-Tejada, P.J.; Girona, J.; Gonzalez-Dugo, V.; Fereres, E. A tool for detecting crop water status using airborne high-resolution thermal imagery. In *Sustainable Irrigation and Drainage V: Management, Technologies and Policies*; WIT Transactions on Ecology and The Environment: Poznan, Poland, 2014; pp. 25–31.
38. Kramer, P.J. *Water Relations of Plants*; Academic Press: New York, NY, USA, 1983.
39. Li, W.D.; Li, S.H.; Yang, S.H.; Yang, J.M.; Zheng, X.B.; Li, X.D.; Yao, H.M. Photosynthesis in response to sink-source manipulations during different phenological stages of fruit development in peach trees: Regulation by stomatal aperture and leaf temperature. *J. Hortic. Sci. Biotechnol.* **2005**, *80*, 481–487.